


RESEARCH

Open Access



CFD analysis in effects of spacer-vane on thermal–hydraulic performance of two-phase flow in annular channel

Satish Kumar Dhurandhar^{1*} , S. L. Sinha¹ and Shashi Kant Verma²

*Correspondence:
satishdhurandhar@gmail.com

¹ Mechanical Engineering
Department, National Institute
of Technology Raipur, Raipur, CG
492010, India

² Mechanical Engineering
Department, National Institute
of Technology Durgapur,
Durgapur, West Bengal 713209,
India

Abstract

Spacer performs a key function in the construction of nuclear rod assembly. It is utilized to ensure the appropriate spacing and firmness of the rods in assembly. In rod bundle structures, spacers are typically incorporated with vanes to promote turbulence and improve heat transfer. The aim of this work is to analyze the impacts of spacer-vane on the thermal–hydraulic performance of two-phase flow in an annular channel. CFD model of an upward flow annular channel with spacer-vane has been developed. In addition, an annular channel model with a spacer but without vane has been generated and modeled in order to examine the impact of the spacer-vane in a two-phase flow. Transient simulations were performed with flow considerations of mass flux 714.4 kg/m²s, liquid temperature 330 K, volume fraction 0.35, heat flux 197.2 kW/m², and atmospheric pressure conditions. CFD results have been validated with experimental data. Results show that the core zone of the annulus gap exhibits the highest level of turbulent intensity, and the outer pipe wall temperature is lower for spacer-vane relative to spacer alone. It is observed that the majority of water vapor is concentrated at the center of the channel in the farthest downstream location.

Keywords: CFD, Spacer-vane, Two phase, Thermal–hydraulic, Annular domain, Turbulent flow

Introduction

Numerous systems that rely on the phenomenon of two-phase flow are prevalent across various industrial sectors, including chemical, petrochemical, and nuclear engineering. Rod bundles, annular channels, and pipes are frequently employed as flow domains in these industrial sectors. In reactor rod bundles, the phenomenon of two-phase flow is extremely complicated due to intricate flow patterns, interface distortion, relative motion between fluids, and strong secondary flow. The precise forecast of thermal–hydraulic characteristics in a two-phase flow within reactor fuel channels relies on a thorough analysis of several factors. These factors include the impacts of grid spacer vanes on the mechanisms of phase interactions (specifically the interfacial area concentration analysis), flow phenomena, and the distribution of flow characteristics for the two-phase fluids (including the analysis for distributions of velocity, volume fraction,

and bubble size). Therefore, the examination of thermal–hydraulic performance in two-phase flow plays an essential part in the effective design of rod bundles equipped with grid spacer-vane and in the safe functioning of the reactor core.

Many researchers have used numerical and experimental methods to predict two-phase thermal–hydraulic performance in nuclear rod applications. Serizawa et al. [1] investigated experimentally the turbulent phenomena of water–air bubbly flow in a vertical pipe. A tracer technique with a concentration of helium gas was used for the analysis of heat and transport of bubbles in two-phase flow. Numerical and experimental analyses of the flow behavior of subcooled boiling in vertical annulus were conducted by Lee et al. [2]. Water and vapor were considered as fluid of two-phase flow, and analyses were performed for different mass fluxes range 476–1061 kg/m²s. Ustinenko et al. [3] developed the methodology using CFD (computational fluid dynamics) to validate the various experimental work performed in two-phase flow by past researchers. Thermal–hydraulic performance was analyzed with constant heat flux in annular channels and pipes.

Ala et al. [4] studied the impacts of partial and complete blockage of the flow passage of the subchannels in nuclear fuel rod bundle for two-phase fluid flow. The authors investigated the blockage effects on void fraction, turbulent intensity, pressure drop, and velocity distributions inside the subchannels at different locations downstream. Chalgeri and Jeong [5] studied the flow regimes transition of two-phase fluid flow in rectangular channels with narrow gaps. Air and water were employed as two-phase fluids inside the domain. They proposed a model for transition criteria and showed good agreement against measurement data. Sadatomi et al. [6, 7] performed experiments on rod bundles having triangular and square arrays for two-phase (air–water) flow. The fluctuation in differences in static pressure between the subchannels of the rod bundle was measured. Turbulent mixing rates were compared for the different arrays used in the experiments and concluded that array configurations of subchannels play an important part in examining the turbulent mixing rate.

Kawahara et al. [8–10] conducted experiments on the rectangular-shaped subchannels for two-phase fluid flow. Water and air flow characteristics visualization was accomplished with the help of acrylic glass. Authors reported that large bubbles have a significant effect on turbulent mixing rate as compared to that of small bubbles, and also, they developed a model for slug flow to predict the effect on turbulent mixing rate.

Dhurandhar et al. [11] presented a thorough review of mixing vane impacts on thermal–hydraulic characteristics for different channel geometries. A detailed review was provided by considering supercritical fluids (as single phase) and different two-phase fluids. Dhurandhar et al. [12–15] performed computer simulations to examine the impacts of spacers and vanes on thermal–hydraulic characteristics of various fluids in a vertical flow annular channel and concluded that spacers and the vanes are significant channel structures for improving heat transfer.

Arai et al. [16] executed an experimental analysis of void fraction in a boiling water reactor for non-heated provisions of the rods. Pressure drop and density distributions along the bundle length were disused. Williams et al. [17] examined two-phase flow patterns experimentally. Bubbly, annular, and slug flow were analyzed at constant pressure in a vertical flow rod bundle. Ren et al. [18] studied the impact of grid spacer and

mixing vane on the phase distribution within rod bundle assembly. Air and water were employed as two-phase fluids. Also, experimental results explained the void fraction distributions in the subchannels.

Drucker et al. [19] explained the heat transfer mechanism in two-phase fluid flow in a tube and fuel rod assembly. Analyses of heat transfer were performed for different ranges of Reynolds numbers. Air and water were employed as two-phase fluids inside the domain, and void fraction distributions were discussed in detail. Li et al. [20] conducted experiments to analyze the heat transfer performance of two-phase fluid flow in a vertical rod bundle assembly. They found that for their test conditions, increasing the system pressure or mass flux will reduce the wall surface superheating degree. Mixing vane effects were studied numerically on the fuel rod assembly for two-phase fluid flow by Xiao et al. [21]. CFD results validation against experimental data was performed. They analyzed the flow and thermal characteristics within the sub-channels of the rod bundle. The authors found that the cross-flow plays an important role in the accumulation of vapor on the fuel rod in the domain.

Yang et al. [22] investigated the impacts of spacer grids, including plastic protrusions, on air–water (two-phase) flow within assembly of an 8×8 array. The downstream turbulence behavior is stronger, and the low-pressure zone is visible behind the grid spacer. Tian et al. [23] conducted tests to measure the pressure drop within rod bundle assembly for a two-phase (air–water) flow. They discussed the turbulent intensity and velocity distributions in the domain. Also, they developed a correlation for a two-phase friction multiplier and tested it successfully.

Hosokawa et al. [24] examined flow behaviors of two phases like liquid velocity, void fraction, and bubble velocity in rod bundle subchannels. The work was done on a lattice with a square shape assembly of 4×4 array having 10-mm rod diameter, 9.1-mm hydraulic diameter, and 1.25 pitch-to-rod diameter ratio, and the authors reported that the acting lift force across bubbles in rod bundle subchannels affects void fraction distributions significantly. Inoue et al. [25] experimentally analyzed the distributions of void fraction within rod bundle. Measurements were performed for normal operating conditions of boiling water reactor rod bundles. An X-ray CT scanner was used to measure the void fractions in the domain.

Based on the aforementioned study of literature, it is inferred that the inclusion of a spacer or grid spacer with vanes has a positive impact on the rate of turbulence mixing and heat transfer improvement. This effect is particularly notable at the spacer location and in the downstream zone of the spacer. Despite the existence of several studies on spacer analysis, the precise forecast of thermal–hydraulic characteristics using computational analysis remains an ongoing area of research for two-phase. This is mainly significant for the design of spacers with varying vane shapes. Moreover, the detailed comparative analysis for the impacts of spacer-vane and spacer alone on thermal–hydraulic performance of two-phase flow in annular channel has received little attention in the literature. Most investigations have been conducted in adiabatic flow conditions. This study presents a novel approach to predicting the thermal–hydraulic performance of two-phase annulus flow with a spacer-vane. The present study examines the impacts of spacer-vane on thermal–hydraulic performance of two-phase flow in annular channels using computational CFD analysis. The Eulerian model was employed to solve the

two-phase fluid flow within a three-dimensional annular channel model. The SST $k-\omega$ mixture turbulence model was utilized for two-phase turbulent flow simulations. Simulations were achieved in ANSYS Fluent for the flow considerations of mass flux $714.4 \text{ kg/m}^2\text{s}$, liquid temperature 330 K , volume fraction 0.35 , heat flux 197.2 kW/m^2 , and atmospheric pressure condition. A detailed investigation was conducted to examine the impacts of spacer-vane on thermal–hydraulic performance of two-phase annulus flow.

Numerical modeling approach

Mathematical equations

The ANSYS Fluent multiphase Eulerian model was used to solve two-phase fluid flow in three-dimensional models of annular channels. Water (liquid) and water vapor were considered as primary and secondary phases, respectively. The governing equations [26] were solved for the two-phase fluid flow during the simulations, which are given as follows:

Continuity equation of phase q

$$\frac{\partial}{\partial t}(\alpha_q \rho_q) + \nabla \cdot (\alpha_q \rho_q \vec{V}_q) = \sum_{p=1}^n (\dot{m}_{pq} - \dot{m}_{qp}) + S_q \tag{1}$$

where \vec{V}_q = velocity of q^{th} phase

\dot{m}_{pq} = mass transfer from p^{th} to q^{th} phase

\dot{m}_{qp} = mass transfer from q^{th} to p^{th} phase

α_q = volume fraction of q^{th} phase

S_q = source term

Momentum equation of phase q

$$\begin{aligned} \frac{\partial}{\partial t}(\alpha_q \rho_q \vec{V}_q) + \nabla \cdot (\alpha_q \rho_q \vec{V}_q \vec{V}_q) &= -\alpha_q \nabla p + \nabla \cdot \bar{\tau}_q + \alpha_q \rho_q \vec{g} \\ &+ \sum_{p=1}^n (\vec{R}_{pq} + \dot{m}_{pq} \vec{V}_{pq} - \dot{m}_{qp} \vec{V}_{qp}) \\ &+ (\vec{F}_q + \vec{F}_{lift,q} + \vec{F}_{wl,q} + \vec{F}_{vm,q} + \vec{F}_{td,q}) \end{aligned} \tag{2}$$

where $\bar{\tau}_q$ = stress–strain tensor of q^{th} phase

$$\bar{\tau}_q = \alpha_q \mu_q \left(\nabla \vec{V}_q + \vec{V}_q^T \right) + \alpha_q \left(\lambda_q - \frac{2}{3} \mu_q \right) \nabla \cdot \vec{V}_q \vec{I} \tag{3}$$

where μ_q = shear viscosity of phase q

λ_q = bulk viscosity of phase q

Energy equation of phase q

$$\frac{\partial}{\partial t}(\alpha_q \rho_q h_q) + \nabla \cdot (\alpha_q \rho_q \vec{u}_q h_q) = \alpha_q \frac{\partial P_q}{\partial t} + \bar{\tau}_q : \nabla \vec{u}_q - \nabla \cdot \vec{q}_q + S_q + \sum_{p=1}^n (Q_{pq} + \dot{m}_{pq} h_{pq} - \dot{m}_{qp} h_{qp}) \tag{4}$$

where h_q = specific enthalpy of q^{th} phase

\vec{q}_q = heat flux

Q_{pq} = heat exchange intensity between p^{th} and q^{th} phases

h_{pq} = interphase enthalpy

Turbulence model

The equations of SST k- ω mixture turbulence model [26] are given as follows:

$$\frac{\partial}{\partial t}(\rho_m k) + \nabla \cdot (\rho_m \vec{V}_m k) = \nabla \cdot \left(\left(\mu_m + \frac{\mu_{t,m}}{\sigma_k} \right) \nabla k \right) + G_{k,m} - Y_{k,m} + S_{k,m} \tag{5}$$

$$\frac{\partial}{\partial t}(\rho_m \omega) + \nabla \cdot (\rho_m \vec{V}_m \omega) = \nabla \cdot \left(\left(\mu_m + \frac{\mu_{t,m}}{\sigma_\omega} \right) \nabla \omega \right) + G_{\omega,m} - Y_{\omega,m} + D_{\omega,m} + S_{\omega,m} \tag{6}$$

where mixture density, $\rho_m = \sum_{i=1}^N \alpha_i \rho_i$

Mixture molecular viscosity, $\mu_m = \sum_{i=1}^N \alpha_i \mu_i$

Mixture velocity, $\vec{V}_m = \frac{\sum_{i=1}^N \alpha_i \rho_i \vec{V}_i}{\sum_{i=1}^N \alpha_i \rho_i}$

Mixture turbulent viscosity, $\mu_{t,m} = \rho_m C_\mu \frac{k}{\omega}$, where $C_\mu = 0.024$ (constant)

The production of turbulence kinetic energy; $G_{k,m}$

$$G_{k,m} = \mu_{t,m} \left(\nabla \vec{V}_m + (\nabla \vec{V}_m)^T \right) : \nabla \vec{V}_m \tag{7}$$

Interfacial forces modeling

Drag force

The interphase momentum transfer between two phases due to the drag force can be obtained via the drag model of Schiller and Naumann model [27]. The drag function f is given as follows:

$$f = \frac{C_D Re}{24} \tag{8}$$

where coefficient of drag (C_D) is given as follows:

$$C_D = \begin{cases} 24(1 + 0.15Re^{0.687})/Re & Re \leq 1000 \\ 0.44 & Re > 1000 \end{cases} \tag{9}$$

The relative Reynolds number for primary phase q and secondary phase p is obtained as follows:

$$Re = \frac{\rho_q |\vec{V}_p - \vec{V}_q| d_p}{\mu_q} \tag{10}$$

where d_p is the bubble diameter of phase p.

Lift force

The lift force acting on a secondary phase p in a primary phase q can be calculated as follows:

$$\vec{F}_{lift} = -C_l \rho_q \alpha_p (\vec{V}_q - \vec{V}_p) \times (\nabla \times \vec{V}_q) \tag{11}$$

where ρ_q = primary phase density

α_p = secondary phase volume fraction

\vec{V}_q and \vec{V}_p = velocity of primary and secondary phase respectively

C_l = lift coefficient

Tomiya lift force model [28] has been used in the simulations to solve the lift coefficient (C_l), which is given as follows:

$$C_l = \begin{cases} \text{Min} [0.288 \tanh (0.121 Re_p, f(Eo'))] & Eo' \leq 4 \\ f(Eo') & 4 < Eo' \leq 10 \\ -0.27 & 10 < Eo' \end{cases} \tag{12}$$

where

$$f(Eo') = 0.00105 Eo'^3 - 0.0159 Eo'^2 - 0.0204 Eo' + 0.474 \tag{13}$$

Eo' is a modified Eotvos number based on the long axis of the deformable bubble, d_h

$$Eo' = \frac{g(\rho_q - \rho_p) d_h^2}{\sigma} \tag{14}$$

$$d_h = d_p (1 + 0.163 Eo^{0.757})^{1/3} \tag{15}$$

$$Eo = \frac{g(\rho_q - \rho_p) d_p^2}{\sigma} \tag{16}$$

where σ = surface tension

g = gravity

d_p = bubble diameter

Wall lubrication force

Wall lubrication force proposed by Antal et al. [29] is given as follows:

$$\vec{F}_{wl} = C_{wl} \rho_q \alpha_p |\vec{V}_q - \vec{V}_p|^2 \vec{n}_w \tag{17}$$

where $|\vec{V}_q - \vec{V}_p|$ = relative velocity between phases

\vec{n}_w = unit normal from wall

C_{wl} = wall lubrication coefficient

Wall lubrication coefficient (C_{wl}) proposed by Antal et al. [29] is given as follows:

$$C_{wl} = \max\left(0, \frac{C_{w1}}{d_b} + \frac{C_{w2}}{y_w}\right) \quad (18)$$

where $C_{w1} = -0.01$ and $C_{w2} = 0.05$ are dimensionless coefficients.

y_w = nearest wall distance

Turbulent dispersion force

The turbulence-induced dispersion force proposed by Lopez de Bertodano model [30] is given as follows:

$$\vec{F}_{td,q} = -\vec{F}_{td,p} = C_{TD}\rho_q k_q \nabla\alpha_p \quad (19)$$

where k_q = primary phase turbulent kinetic energy

$\nabla\alpha_p$ = secondary phase volume fraction gradient

$C_{TD} = 1$, turbulent dispersion constant

Virtual mass force:

The equation for virtual or added mass force [26] is given as follows:

$$\vec{F}_{vm,q} = 0.5\alpha_p\rho_q\left(\frac{d_q\vec{V}_q}{dt} - \frac{d_p\vec{V}_p}{dt}\right) \quad (20)$$

where $\frac{d_q}{dt}$ = time derivative of phase material

Geometry development and boundary details

CFD model of an upward flow annular channel with spacer-vane has been developed. Additionally, an annular channel model with a spacer but without vane has been generated and modeled to study the impacts of spacer-vane in a two-phase flow. Figure 1 a, b, c, and d shows the geometry details of a three-dimensional annular channel with spacer-vane. The blockage ratio of spacer located at the center of the annular channel is assumed to be 0.4. Vanes have been positioned on the spacer tip in the flow direction, and the vane dimensions are shown in Fig. 2. The vane angle is taken as 7° with the flow direction. Table 1 represents the dimensions of simulation geometry.

In the present work, an Eulerian model was used for two-phase fluid (water and water vapor mixture) formulation. Transient simulations were performed with time step size of 0.005 s and total number of time steps of 600. Temperature, hydraulic diameter, volume fraction, mass flux, and turbulent intensity were applied at the domain inlet. The saturation temperature of water has been set as 373.15 K at atmospheric pressure. Constant pressure was employed at the domain outlet. Adiabatic and constant heat flux criteria were employed on the inner and outer pipes, respectively.

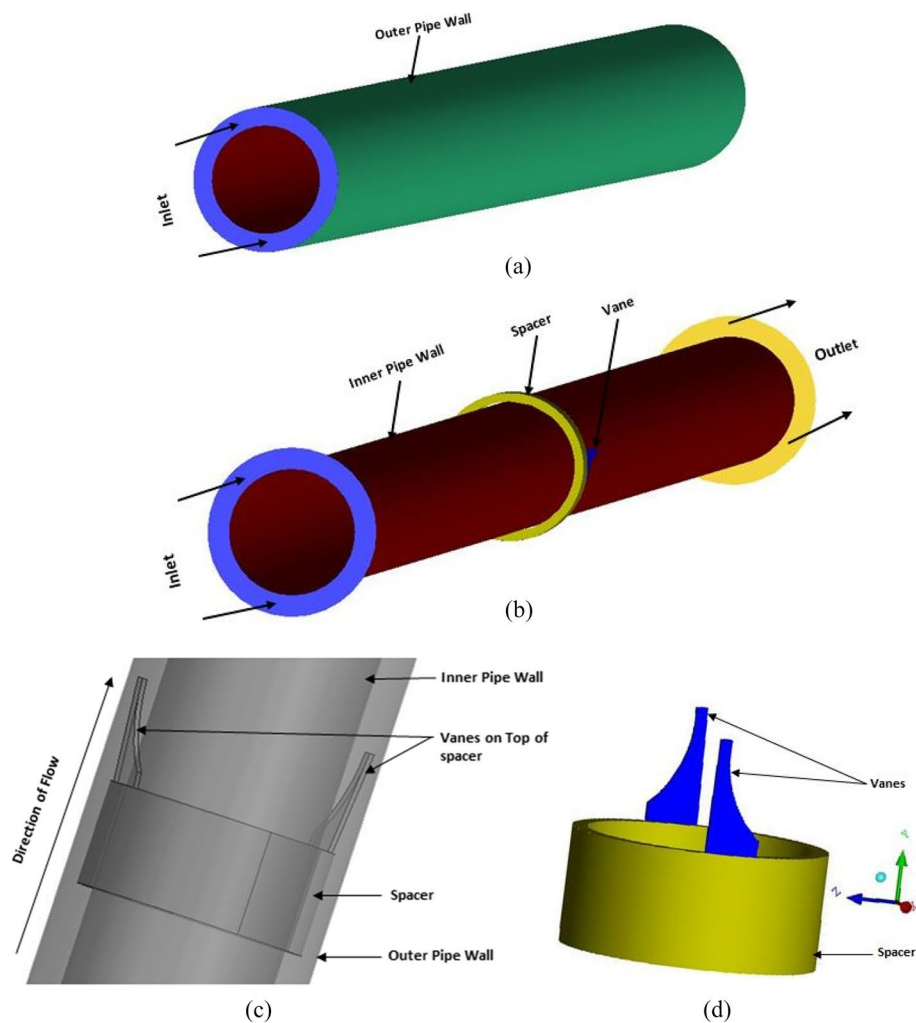


Fig. 1 Geometry details. **a** A three-dimensional annular channel, **b** an annular channel with its boundaries, **c** channel with spacer-vane, and **d** vane on the spacer tip

Smooth wall with no-slip criteria was employed on the walls for momentum equation. Table 2 provides the details of boundary condition.

Mesh model and mesh independence

Mesh independence analysis was executed employing three distinct mesh models. Meshes 1, 2, and 3 possess element counts of 1.9, 1.6, and 1.3 million, respectively. The unstructured tetrahedron mesh models were generated employing ICEM CFD. Mesh was generated by specifying the size of global element with a fixed scaling factor. Mesh refinement was accomplished by retaining distinct sizes of elements on the vane, spacer, and inner-outer pipe surfaces. In order to effectively represent the heat transfer phenomenon, prismatic layers of elements were built close to pipe walls. The initial layer's height on the pipe surface was kept low enough; thus, y^+ is smaller than 1. An expansion ratio of 1.2 was employed among layers. Figure 3 represents a mesh model for the geometry used in the present analysis. Figures 3 a and b represents the

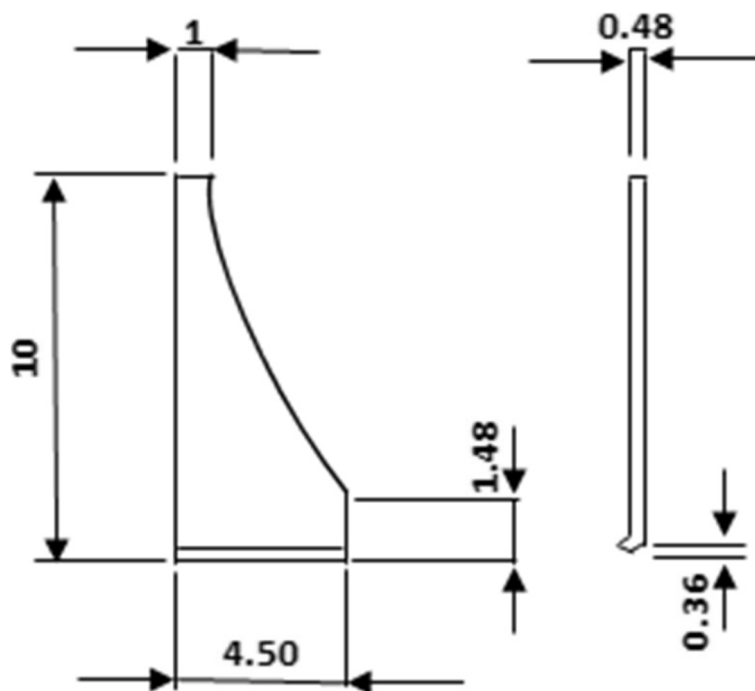


Fig. 2 Dimension of vane in millimeter

Table 1 Dimensions of simulation geometry

Geometry parameters	Value
Inner pipe radius	9.5 mm
Outer pipe radius	12.5 mm
Annulus gap	3 mm
Channel length	1000 mm
Hydraulic diameter of channel	6 mm
Length of spacer	10 mm

Table 2 Details of boundary condition

Boundary	Properties and physical conditions
Inlet	Mass flux = 714.4 kg/m ² .s Water temperature = 330 K Diameter of water vapor = 0.01 mm Water vapor temperature = 373.15 K Volume fraction = 0.35 Turbulence Intensity = 5% Hydraulic diameter = 0.006 m
Outlet	Constant pressure = 1 atm Water and water vapor temperature = 373.15 K
Inner pipe	Adiabatic wall
Outer pipe	Constant heat flux = 197.2 kW/m ²

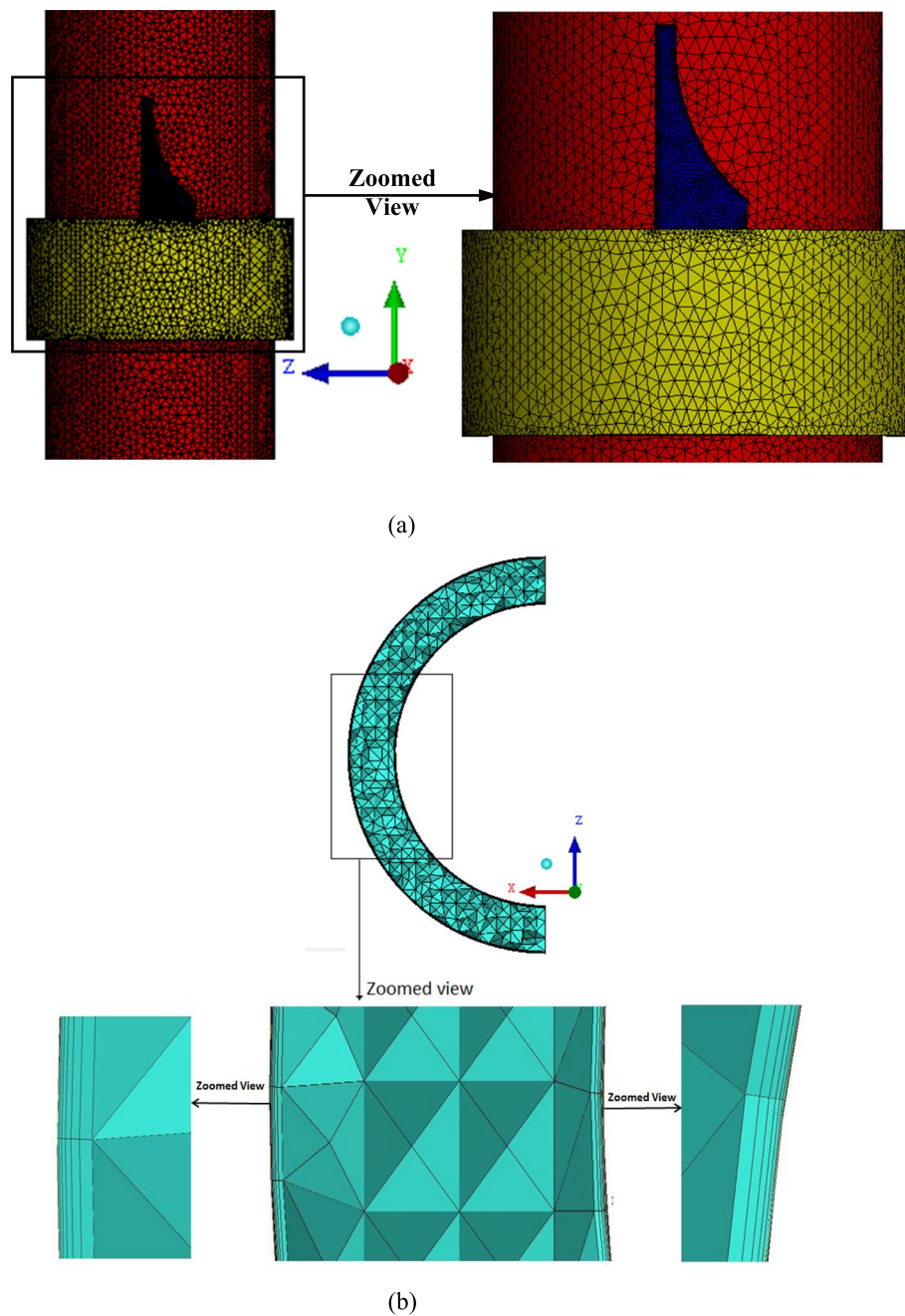


Fig. 3 Mesh model. **a** Surface mesh on inner pipe with spacer-vane and **b** volume mesh at annulus gap

surface and volume mesh over the inner pipe with spacer-vane and at the annulus gap, respectively.

Mesh independence analysis was executed in an annular channel with spacer-vane. The dimensions of the annular channel and flow parameters for mesh independence analysis are given in Tables 1 and 2, respectively. Eulerian model was used to solve the two-phase fluid (water and water vapor) flow. The simulation was accomplished using SST $k-\omega$ mixture turbulence model. The tangential velocity distributions of liquid in radial coordinates for three mesh models are displayed in Fig. 4.

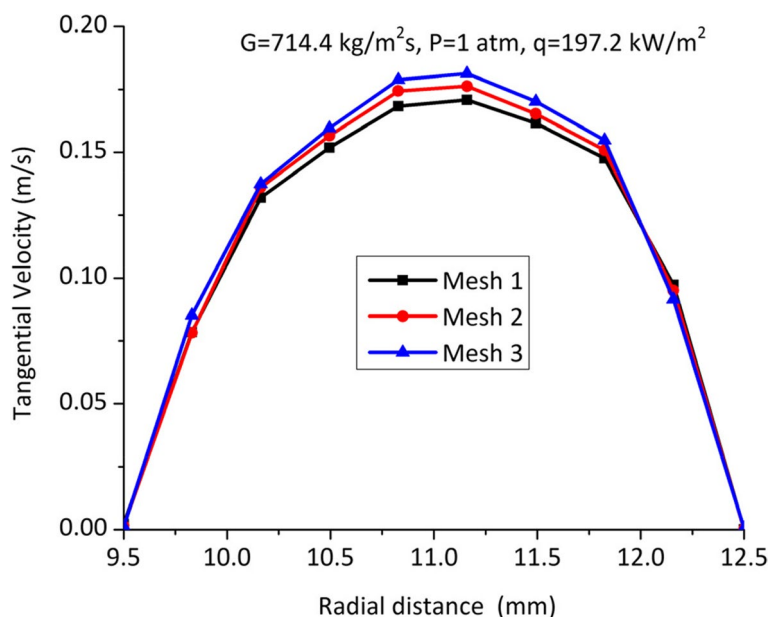


Fig. 4 Mesh independence analysis for annular channel with spacer-vane

Table 3 Numerical percentage deviation of mesh

Mesh	Average percentage deviation w.r.t. Mesh 2
Mesh 1	0.23%
Mesh 2	Selected
Mesh 3	0.26%

The tangential velocities were taken at 460 mm from channel inlet, which is over 40 times of the hydraulic diameter to avoid entrance effect [31]. Hydraulic diameter of the annular channel is 6 mm. Based on the comparison made for the tangential velocity distributions (Fig. 4), mesh 2 was adopted for further numerical analysis as the variation of tangential velocities is less than 0.3% compared to the other two mesh models, i.e., meshes 1 and 3 (it is per the authors consideration). Table 3 shows the numerical percentage deviation of meshes 1 and 3 with respect to mesh 2.

Methods

The multiphase Eulerian model was applied to solve two-phase (water — primary phase and vapor — secondary phase) fluid flow in a three-dimensional model of annular channel. The time step size was taken as 0.005 s for the present transient simulations. The phase-coupled SIMPLE algorithm was employed to couple the velocity and pressure. The finite volume method is the basis of this algorithm. The value of the residuals was specified as 10^{-6} to get converged results for the turbulence model and governing equations. The residuals were achieved using a first-order upwind discretization scheme. The equation for volume fraction was solved by the QUICK scheme. The precision of the results is confirmed by these algorithms and the criteria for residuals to determine the

convergence of the solution. During simulation, the values for under-relaxation were reduced for better convergence of solutions. The convergence was verified with the flux report of net mass flow rate from inlet and outlet boundaries of the domain. Also, the gravity influence was specified for the accuracy of numerical results.

CFD results validation and adoption of turbulence model

The simulation was accomplished in ANSYS Fluent for CFD results validation. Data from an experiment executed by Serizawa et al. [1] was used for CFD results validation. Model dimensions and boundary parameters for CFD validation are identical to an experiment executed by Serizawa et al. [1]. The CFD model used for the validation is shown in Fig. 5. It is a vertical pipe, and the model dimensions are as follows: the diameter and length are 0.06 m and 2.15 m, respectively. The simulation was performed for two-phase fluid (water–air) flow with flow parameters of liquid superficial velocity as 1.03 m/s, gas velocity as 0.151 m/s, bubble diameter as 4 mm, and atmospheric pressure condition. The turbulence models, such as standard $k-\epsilon$ and SST $k-\omega$, were examined to analyze flow performance of this CFD model. Figure 6a and b shows the comparative results for radial distributions of void fraction and liquid velocity obtained from CFD and the experiment, respectively. The radial distributions of void fraction and liquid velocity were taken on line L1, which is at 1.8 m from pipe inlet (Fig. 5). Figure 6a shows that the peak of void fraction is close to the pipe wall because of the lift force acting on gaseous phase and the higher bubble diameter. Figure 6b shows that the liquid velocity is maximum at the center of the pipe and zero at the pipe wall. Tables 4 and 5 represent the uncertainty in CFD results for void fraction and liquid velocity distributions compared with experiment, respectively. It is obvious from Fig. 6a and b that the CFD results of void fraction and liquid velocity determined by turbulence model of SST $k-\omega$ were a better match to experimental data than the standard $k-\epsilon$. Thus, the impacts of spacer-vane were analyzed by adopting the SST $k-\omega$ for subsequent simulations of CFD in the annular channel. Moreover; several researchers have found that the SST $k-\omega$ is more appropriate for thermal–hydraulic analysis within nuclear rod bundle assemblies compared to other turbulence models [32–38]. Based on the previous research works conducted by several researchers [32–38] for flow thermal characteristics analysis in nuclear fuel channels, the authors examined the SST $k-\omega$ and the standard $k-\epsilon$ in the present work. The SST $k-\omega$ turbulence model predicted more accurately than the standard $k-\epsilon$ model.

Results and discussion

In this section, the thermal–hydraulic performance of two-phase flow in annular channels with spacer-vane was discussed. Simulation results were produced for the flow considerations of mass flux $714.4 \text{ kg/m}^2\cdot\text{s}$, liquid temperature 330 K, volume fraction 0.35, heat flux 197.2 kW/m^2 , and at atmospheric pressure condition. The parametric plot for convergence of the present simulation in an annular channel with spacer-vane is shown in Fig. 7.

Effect of spacer-vane on velocity and pressure distributions

The tangential and radial velocity distributions of liquid in radial coordinates have been presented in Figs. 8 and 9, respectively. The velocity distributions and distance in radial

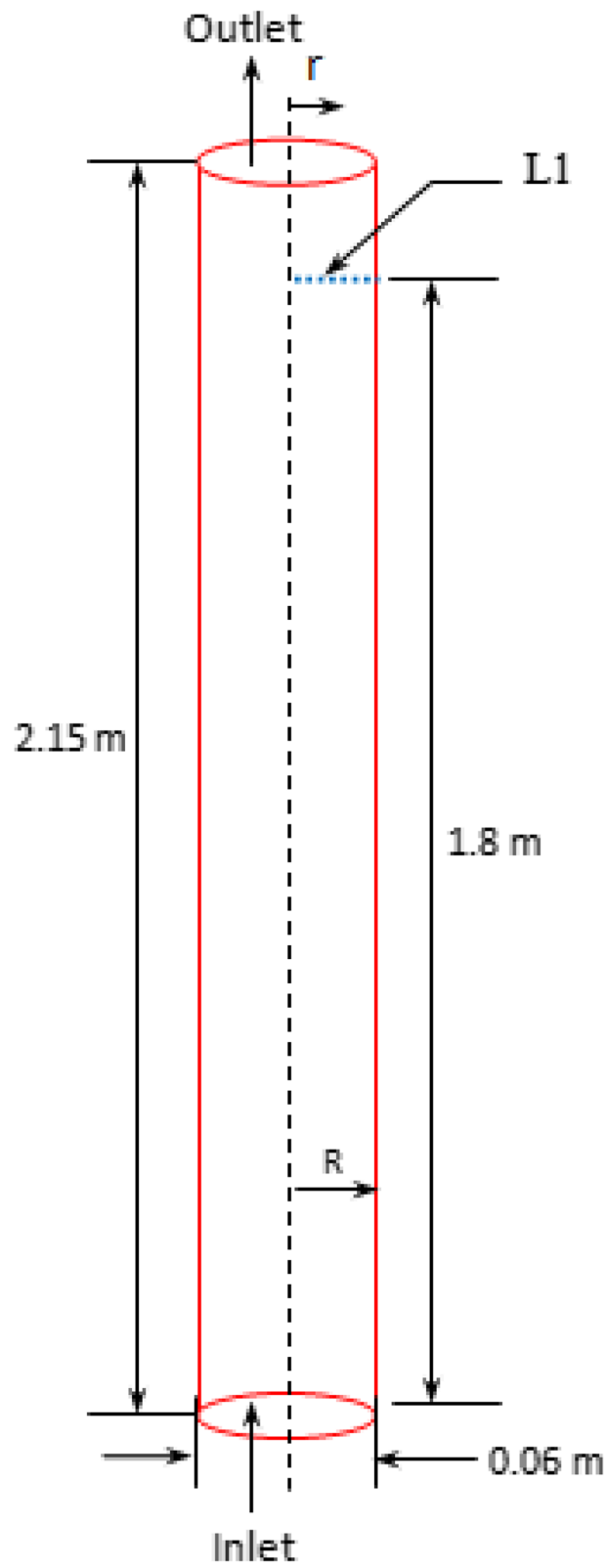
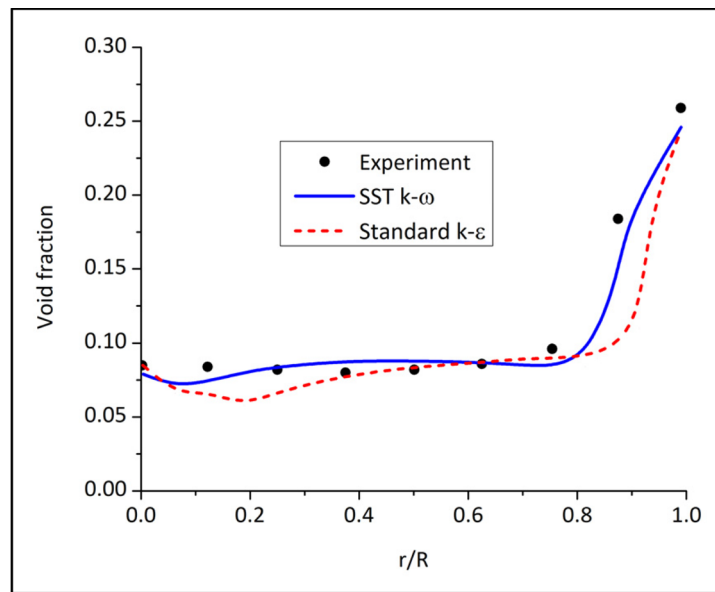
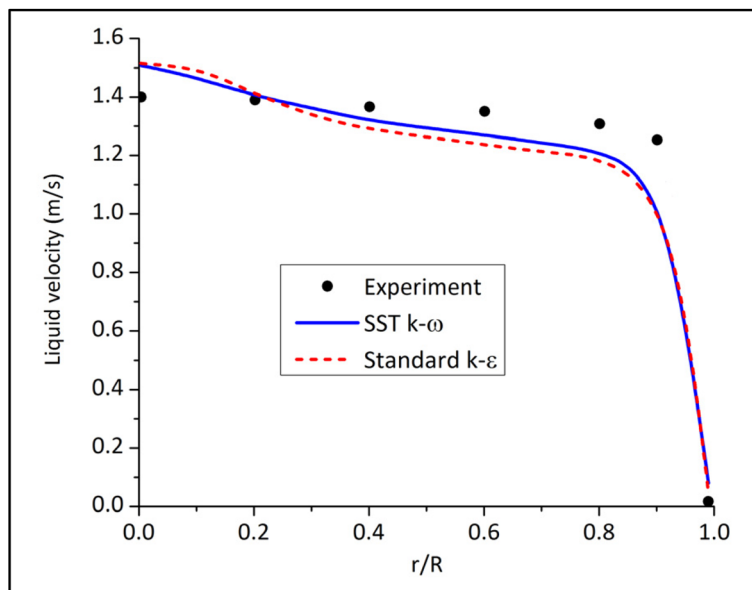


Fig. 5 Computational model used for validation



a). (Void fraction distribution-CFD validation.



(b). Liquid velocity distribution-CFD validation.

Fig. 6 a Void fraction distribution-CFD validation. b Liquid velocity distribution-CFD validation

coordinates are shown on the ordinate and abscissa, respectively. The velocity distributions have been taken at different sites ($X/D = 1, 2, 5, 20, 30, 40,$ and 50) in downstream from the spacer tip. X and D represent the downstream distance from spacer tip and a hydraulic diameter, respectively. Figure 8 represents that the tangential velocity magnitude is significantly improved near the wall of outer pipe in the downstream area near the spacer tip (at $X/D = 1$). This improved tangential velocity is because of the spacer

Table 4 Uncertainty in CFD results of volume fraction with experiment

CFD analysis	Average percentage deviation
SST k- ω	0.87%
Standard k- ϵ	1.98%

Table 5 Uncertainty in CFD results of liquid velocity with experiment

CFD analysis	Average percentage deviation
SST k- ω	1.12%
Standard k- ϵ	1.31%

influence as it decreases the area of flow. The tangential velocity gradually reduces adjacent to the outer pipe wall further downstream from the spacer tip (i.e., $X/D=2$ and 5) due to the recovery of flow area [36]. It is obvious from Fig. 8 that from $X/D=20$ onwards downstream, the flow has become fully developed since the variations in the flow velocity profiles are negligible along the flow direction and the spacer effects are negligible. Also, the turbulence induced by the spacer-vane in the flow greatly dies down from $X/D=20$ onwards due to the axial decay of vortices, which appeared due to the presence of the spacer-vane in the flow domain.

Similarly, Fig. 9 shows that the radial velocity magnitude is maximum near the wall of outer pipe which is around 0.8 m/s for location of $X/D=1$. Further downstream up to $X/D=5$, the radial velocity reduces gradually near the outer pipe wall due to the recovery of flow area, and $X/D=20$ onwards in downstream of the spacer effects disappear [36].

Figure 10 a and b represents the axial velocity contour of liquid for spacer only (without vane) and spacer-vane in annular channel, respectively. The velocity contour has been taken on the midplane of the channel annulus gap. The spacer serves the purpose of decreasing domain flow area by acting as a flow blockage. Decreased domain flow area increases flow velocity. The spacer's vane further increases flow velocity considerably in the downstream area near the spacer. Figure 10 clearly shows that the maximum velocity magnitude exceeds 1.3 m/s with spacer-vane, which is higher than that of spacer alone in the annular channel. Enhanced flow velocity contributes significantly to reducing the channel wall temperature, which enhances heat transfer performance.

Figure 11 shows the axial velocity distribution of liquid in radial coordinates of the annular channel with spacer-vane. Figure 11 shows that the axial velocity magnitude is maximum near the wall of outer pipe which is around 1.1 m/s for location of $X/D=1$. This enhanced velocity (for $X/D=1$) is because of the spacer influence as it decreases the area of flow. Due to the recovery of flow area, the velocity gradually reduces near the wall of outer pipe in downstream from spacer tip (i.e., $X/D=2$ and 5). Further downstream, the flow has become fully developed [36].

Figure 12 shows the dynamic pressure distribution of liquid. The dynamic pressure magnitude is maximum near the outer pipe wall which is about 650 Pa for location

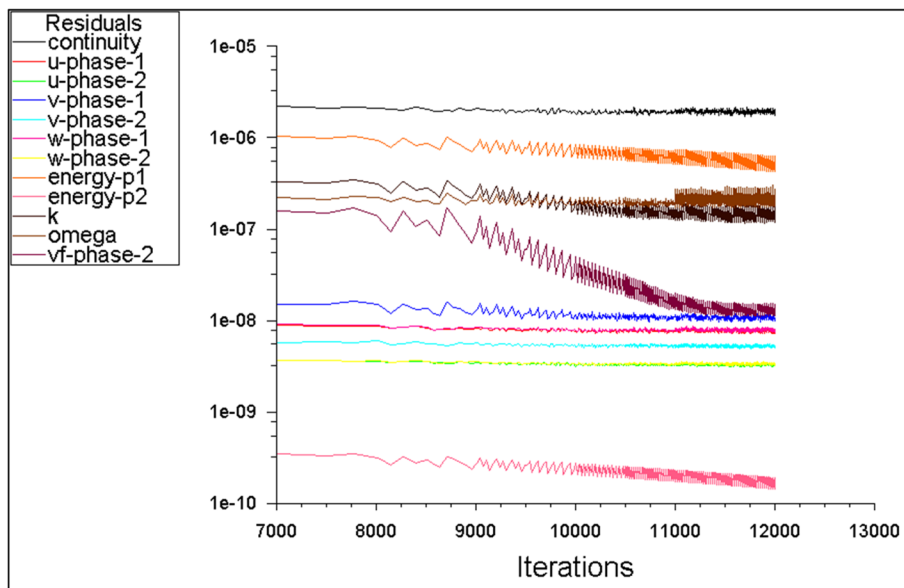


Fig. 7 Convergence plot for the present simulation

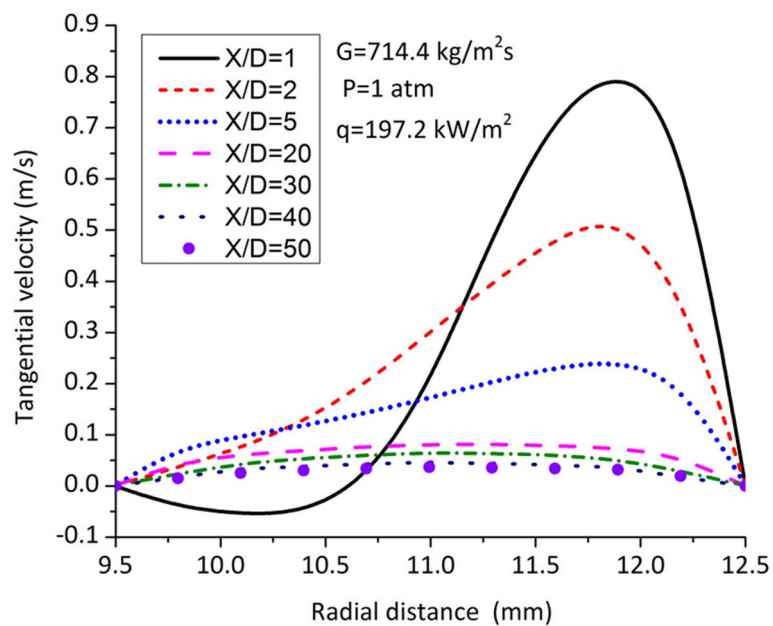


Fig. 8 Tangential velocity distribution of liquid for spacer-vane annular channel

of $X/D=1$. The dynamic pressure increased near the wall of outer pipe due to the augmented flow velocity near spacer downstream. The difference in dynamic pressure between the locations $X/D=1$ and 2 is observed as 250 Pa at radial distance of 12 mm (near the wall of outer pipe). Further downstream, up to $X/D=5$, the dynamic pressure reduces gradually near the outer pipe wall, and then the spacer effects are observed to be negligible ($X/D=20$ onwards).

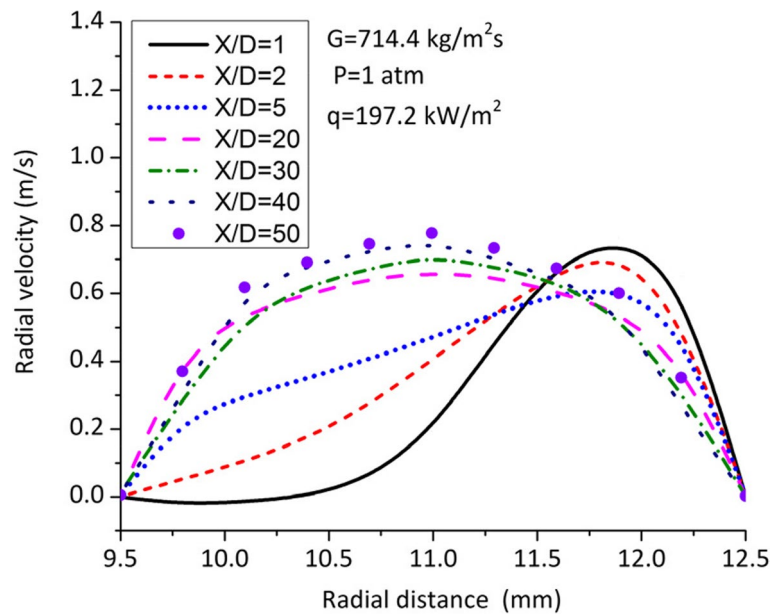


Fig. 9 Radial velocity distribution of liquid for spacer-vane annular channel

Effect of spacer-vane on turbulent intensity

Figure 13 a and b shows the turbulent intensity contour of the mixture for spacer only (without vane) and spacer-vane in annular channel, respectively. The contour of turbulent intensity has been taken on the midplane of the channel which is symmetry from the concentric axis of annular channel. The midplane has been created in annulus gap along the channel length. The maximum turbulent intensity is observed in the core zone of the annulus gap, which is over 16%. This enhanced turbulent intensity in the annulus gap is about 11% higher than the turbulent intensity specified at the inlet of channel. The magnitude of turbulent intensity is observed to be greater using spacer-vane compared to spacer alone in downstream of the channel. Additionally, the effect of vane on turbulent intensity is noticed up to the farthest downstream from the spacer tip compared to spacer alone. This prolonged effect of turbulent intensity in the annulus gap enhances the heat transfer rate in the channel.

Figure 14 shows the turbulent intensity distribution of the mixture in radial coordinates. The distribution has been taken at different sites ($X/D=1, 2, 5, 20, 30, 40,$ and 50) in downstream from the spacer tip. Figure 14 clearly shows that near the spacer tip ($X/D=1, 2,$ and 5) downstream, the turbulent intensity magnitudes are higher at the core zone [39] (at radial distance = 11 mm) of the annulus gap, and the turbulent intensities are again improved significantly near the wall of outer pipe due to spacer influence. The spacer provides a flow blockage and yields vortices behind the spacer downstream. These vortices increase the turbulent mixing in the core zone of the annulus gap, and thus, the turbulent intensity magnitudes are higher at the core zone of the annulus. Maximum turbulent intensity is observed about 14% at the core zone for location of $X/D=2$. Also, Fig. 13b clearly shows that the turbulent intensity magnitude exceeds 16% in the core zone of the annulus gap for location of $X/D=3$. Further, from $X/D=20$ onwards downstream, the turbulent intensity variations are noticed as negligible.

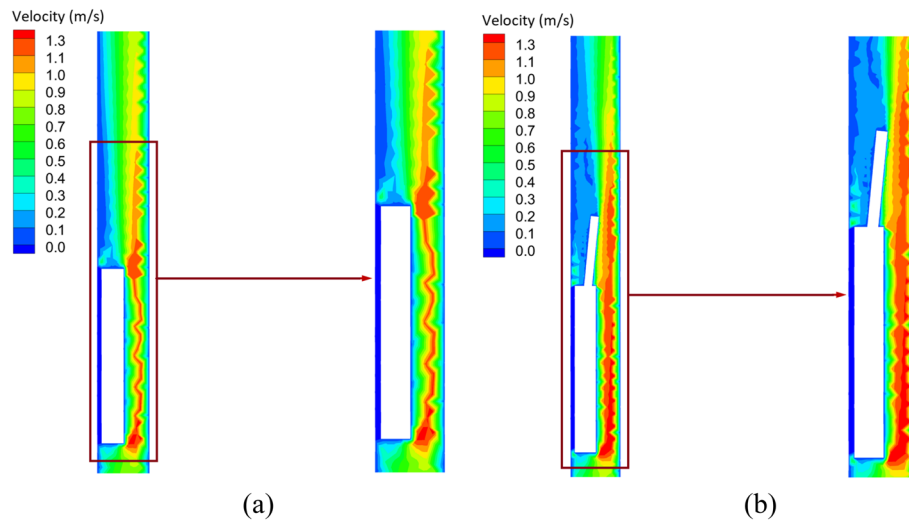


Fig. 10 Axial velocity contour of liquid **a** spacer only and **b** spacer-vane

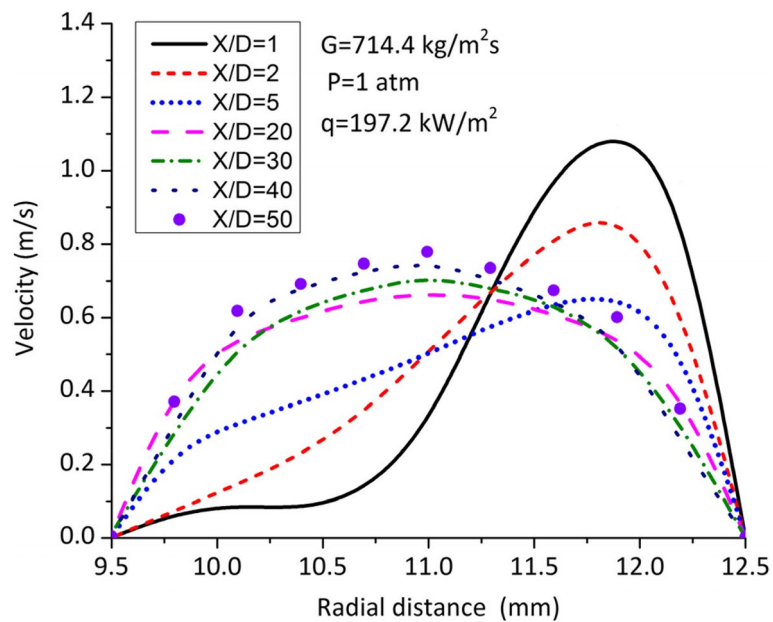


Fig. 11 Axial velocity distribution of liquid for spacer-vane annular channel

Effect of spacer-vane on temperature distributions

Figure 15 a and b shows the temperature contour of liquid for spacer only (without vane) and spacer-vane in annular channel, respectively. The contour has been taken on the midplane which is created in annulus gap along the channel length. Figure 15 a and b clearly shows that near the spacer tip downstream, the temperature magnitude is less near the wall of outer pipe using spacer-vane compared to spacer alone in the channel. The spacer’s vane further enhances the turbulent mixing in the downstream area near spacer; thus, the drop in temperature is observed to be greater using spacer-vane

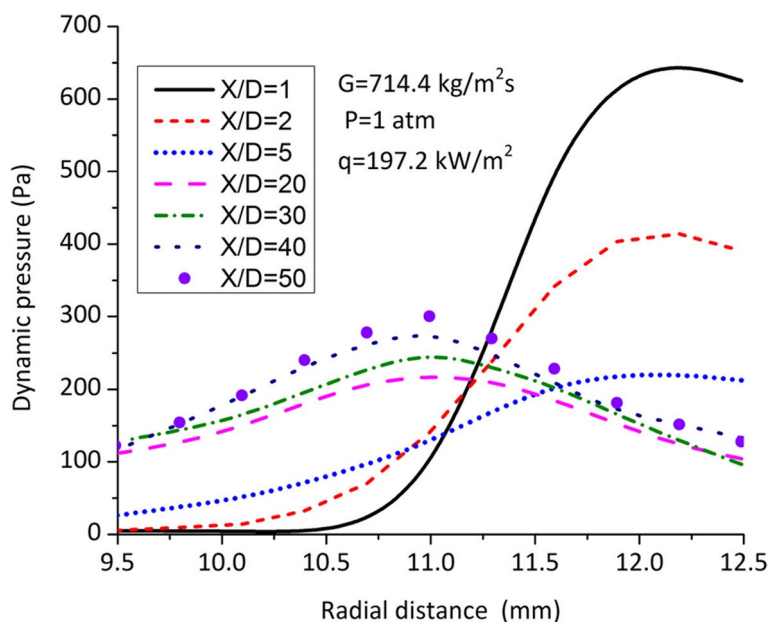


Fig. 12 Dynamic pressure distribution of liquid for spacer-vane annular channel

compared to spacer alone [12]. In the downstream area near the spacer tip, the temperature magnitude is observed in the range of 365 to 373 K near the wall of outer pipe using spacer-vane. Hence, it is obvious that the spacer’s vane further reduces the wall temperature significantly near the spacer downstream.

Figure 16 shows the temperature distribution of liquid in annular channel with spacer-vane. The temperature magnitude is minimum near the wall of outer pipe, which is about 365 K for location of $X/D=1$. Due to the formation of vortices, the turbulent mixing is predominant in the downstream area near the spacer. Turbulent mixing of fluid enhances the turbulence kinetic energy, which causes a reduction in temperature near the spacer downstream [12]. Further downstream, a gradual increase in temperature is observed due to the axial decay of vortices [40]. In downstream, the temperature magnitude increases gradually near the wall of outer pipe and is observed as 375 K for $X/D=5$ and about 395 K for $X/D=50$.

Effect of spacer-vane on volume fraction

Figure 17 represents the volume fraction distribution of water vapor in radial coordinates of the annular channel with spacer-vane. Figure 17 shows that the maximum volume fraction of vapor is about 0.44 (near the spacer tip, i.e., at $X/D=1$ to 5) at a radial distance 11.7 mm from inner pipe wall and then gradually decreases to a minimum at the outer pipe wall. When the flow has fully developed, i.e., $X/D=20$ onwards, the maximum volume fraction (about 0.45 at $X/D=50$) is noticed at the center zone of the annulus gap (i.e., at a radial distance of 11 mm). It is observed that in the farthest downstream, most of the water vapor is present at the core of the annulus gap. The peak of the volume fraction is observed at the core of the annulus gap due to the higher water vapor input (0.35) at the inlet [1] and the small size (diameter 0.01 mm) of the water vapor

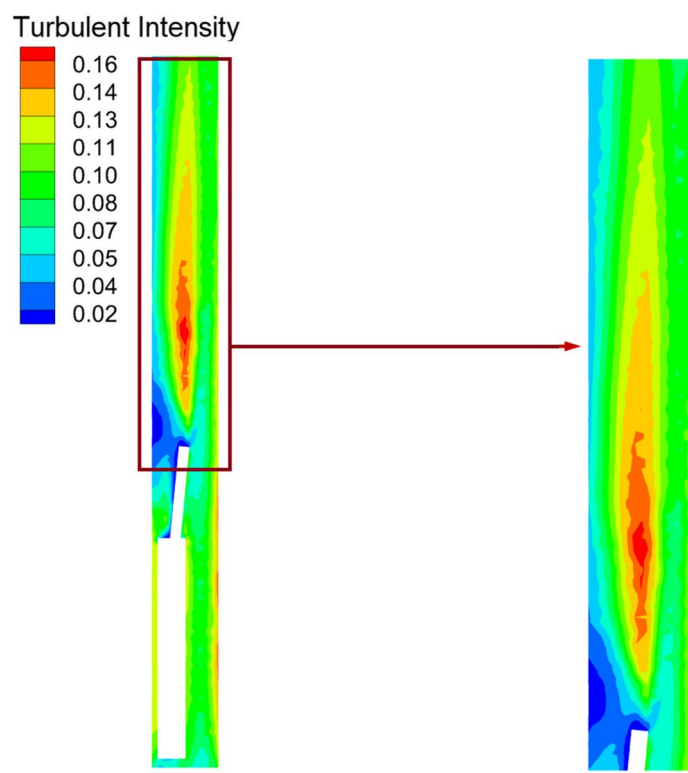
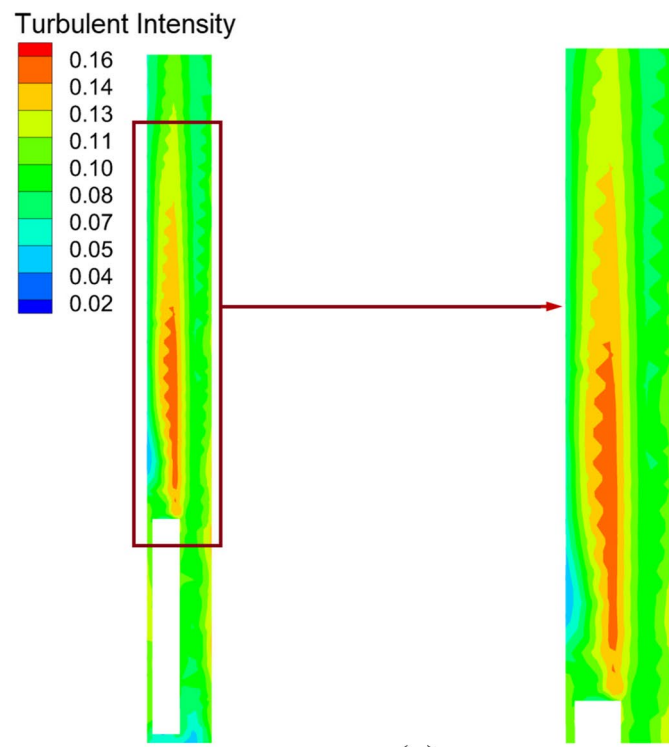


Fig. 13 Turbulent intensity contour of the mixture **a** spacer only (without vane) and **b** spacer-vane

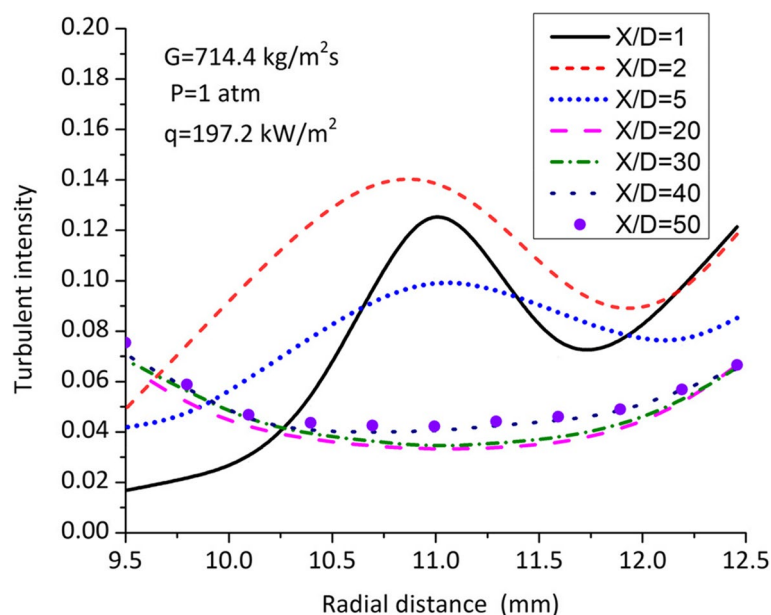


Fig. 14 Turbulent intensity distribution of the mixture for spacer-vane annular channel

bubbles used in the flow field. The minimum volume fraction of water vapor at the outer pipe wall is favorable to enhance the heat transfer rate from the channel wall.

Conclusions

A detailed investigation was conducted to examine the impacts of spacer-vane on thermal–hydraulic performance of two-phase annulus flow. Additionally, an annular channel model with a spacer but without vane was generated and modeled in order to examine the impact of the spacer-vane in a two-phase flow. The multiphase Eulerian model was applied to solve two-phase (water — primary phase and vapor — secondary phase) fluid flow in a three-dimensional model of annular channel. Simulation results were produced for the flow considerations of mass flux $714.4 \text{ kg/m}^2\text{s}$, liquid temperature 330 K , volume fraction 0.35 , heat flux 197.2 kW/m^2 , and at atmospheric pressure condition. The simulation was accomplished using SST $k-\omega$ mixture turbulence model. The impacts of spacer-vane on thermal–hydraulic performance of two-phase annulus flow were studied, and the conclusions are as follows:

- Maximum turbulent intensity is observed in the core zone of annulus gap, which is over 16%. The augmented turbulent intensity in the annulus gap is approximately 11% higher than the turbulent intensity indicated at the channel's inlet.
- The velocity magnitude near the wall of outer pipe is significantly improved in the downstream area near the spacer tip. This improved velocity is because of the spacer influence as it decreases the area of flow.
- Enhanced flow velocity plays a significant role in reducing the wall temperature of channel, and hence, it enhances the heat transfer performance.

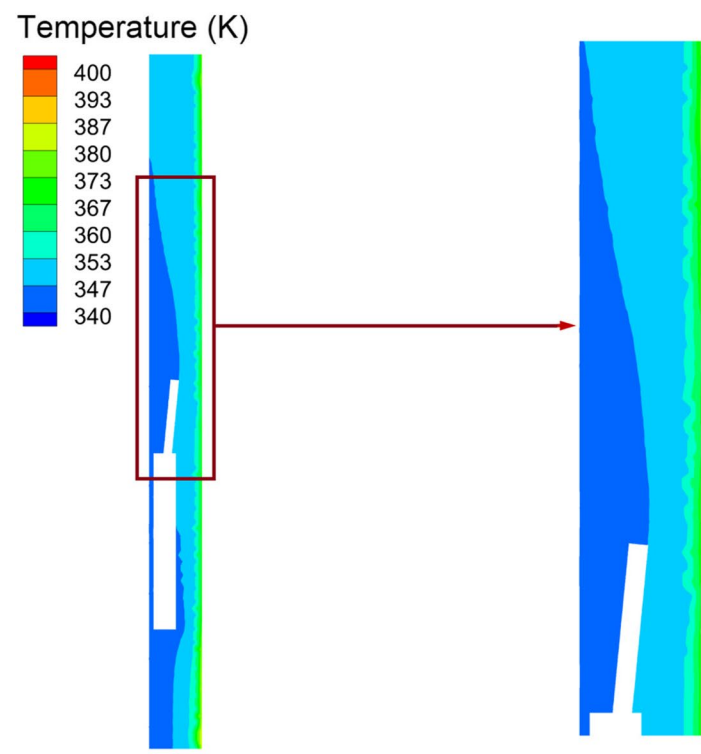
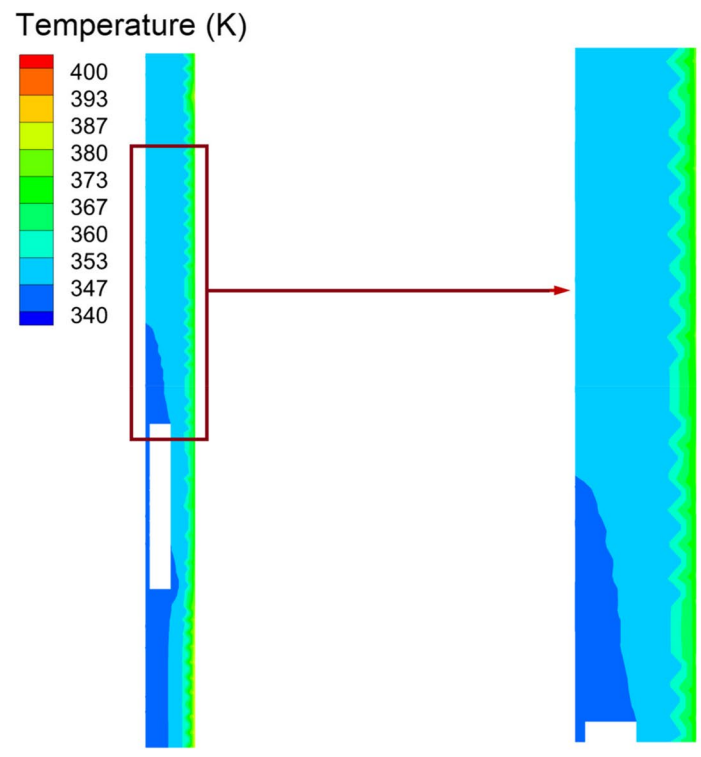


Fig. 15 Temperature contour of liquid a spacer only (without vane) and b spacer-vane

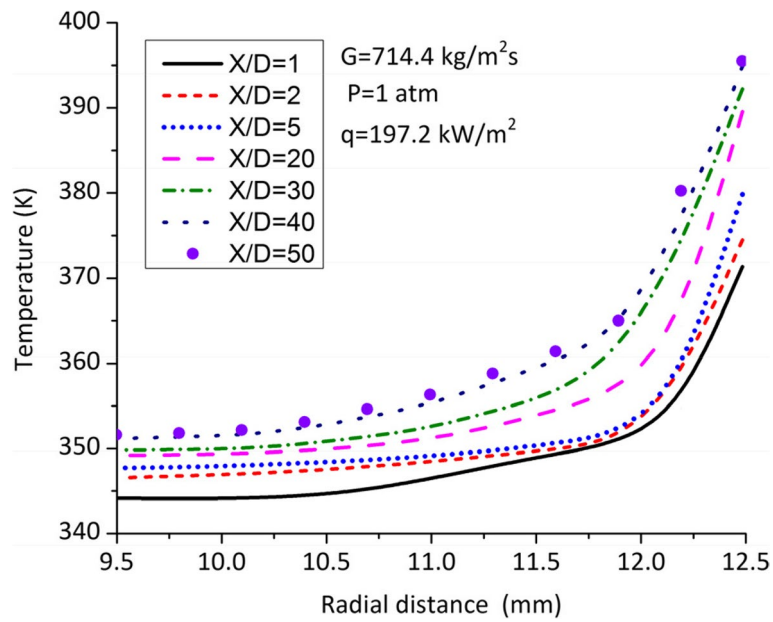


Fig. 16 Temperature distribution of liquid for spacer-vane annular channel

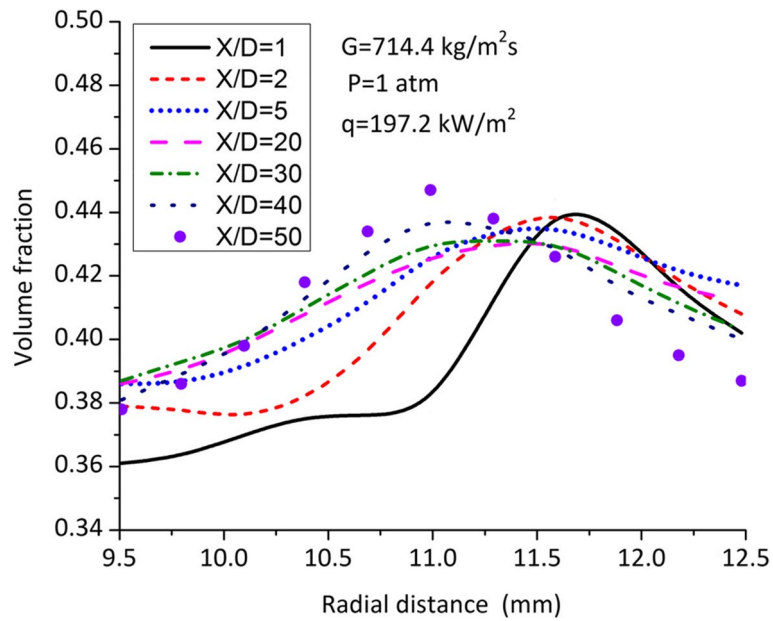


Fig. 17 Volume fraction distribution of water vapor for spacer-vane annular channel

- $X/D = 20$ onwards in downstream, the flow has become fully developed, and the variations in flow parameters are negligible.
- Near the spacer tip downstream, the temperature magnitude is observed to be less near the wall of outer pipe using spacer-vane compared to spacer alone in the channel.

- Due to the small size of water vapor used in the flow field, most of the water vapor is present at the core of the annulus gap in farthest downstream of the channel. The volume fraction of water vapor is observed as minimum at the outer pipe wall, which is favorable to increase the heat transfer rate from the channel wall.

Abbreviations

CFD	Computational fluid dynamics
CT	Computed tomography
SST	Shear stress transport
SIMPLE	Semi-implicit method for pressure-linked equations
QUICK	Quadratic upstream interpolation for convective kinematics

Acknowledgements

The authors acknowledge the cooperation and support extended by the authorities of the National Institute of Technology Raipur for the present work.

Authors' contributions

SKD, SLS, and SKV worked on the conceptualization, methodology, and software implementation for the CFD simulation of the present work. SKD and SKV performed the validation of the work with previous experimental work. SKD compiled graphs and contour related to the CFD simulation results. SKD prepared the original draft and wrote the manuscript. SLS and SKV supervised the study and helped in the reviewing and editing of the manuscript. All authors have read and approved the manuscript.

Funding

The authors declare that they receive no funding.

Availability of data and materials

The datasets used and analyzed during the current study are available from the corresponding author upon reasonable request.

Declarations

Competing interests

The authors declare that they have no competing interests.

Received: 27 October 2023 Accepted: 31 May 2024

Published online: 08 June 2024

References

1. Serizawa A, Kataoka I, Michiyoshi I (1975) Turbulent structure of air-water bubbly flow-II. Local Properties. *Int J Multiphase Flow* 2:235–246. [https://doi.org/10.1016/0301-9322\(75\)90012-9](https://doi.org/10.1016/0301-9322(75)90012-9)
2. Lee TH, Park GC, Lee DJ (2002) Local flow characteristics of subcooled boiling flow of water in a vertical concentric annulus. *Int J Multiphase Flow* 28:1351–1368. [https://doi.org/10.1016/S0301-9322\(02\)00026-5](https://doi.org/10.1016/S0301-9322(02)00026-5)
3. Ustinenko V, Samigulin M, Ilolev A, Lo S, Tentner A, Lychagin A, Razin A, Girin V, Ye V (2008) Validation of CFD-BWR, a new two-phase computational fluid dynamics model for boiling water reactor analysis. *Nucl Eng Des* 238:660–670. <https://doi.org/10.1016/j.nucengdes.2007.02.046>
4. Ala AA, Tan S, Qiao S, Shiru GA (2023) Simulation of the effect of partial and total blockage of a sub-channel on two-phase flow through a 5 x 5 square rod bundle. *Prog Nucl Energy* 155:104514. <https://doi.org/10.1016/j.pnucene.2022.104514>
5. Chalgeri VS, Jeong JH (2022) Flow regime transition criteria for vertical downward two-phase flow in rectangular channel. *Nucl Eng Technol* 54(2):546–553. <https://doi.org/10.1016/j.net.2021.08.014>
6. Sadatomi M, Kawahara A, Kano K, Sumi Y (2004) Single and two phase turbulent mixing rate between adjacent subchannels in a vertical 2x3 rod array channel. *Int J Multiphase Flow* 30(5):481–498. <https://doi.org/10.1016/j.ijmultiphaseflow.2004.03.001>
7. Sadatomi M, Kawahara A, Kano K, Tanoue S (2004) Flow characteristics in hydraulic equilibrium two-phase flows in a vertical 2x3 rod bundle channel. *Int J Multiphase Flow* 30(9):1093–1119. <https://doi.org/10.1016/j.ijmultiphaseflow.2004.05.012>
8. Kawahara A, Sato Y, Sadatomi M (1997) The turbulent mixing rate and the fluctuations of static pressure difference between adjacent subchannels in a two-phase subchannel flow. *Nucl Eng Des* 175(1–2):97–106. [https://doi.org/10.1016/S0029-5493\(97\)00166-0](https://doi.org/10.1016/S0029-5493(97)00166-0)

9. Kawahara A, Sadatomi M, Tomino T, Sato Y (2000) Prediction of turbulent mixing rates of both gas and liquid phases between adjacent subchannels in a two-phase slug-churn flow. *Nucl Eng Des* 202(1):27–38. [https://doi.org/10.1016/S0029-5493\(00\)00300-9](https://doi.org/10.1016/S0029-5493(00)00300-9)
10. Kawahara A, Sadatomi M, Kudo H, Kano K (2006) Single and two phase turbulent mixing rate between subchannels in triangle tight lattice rod bundle. *JSM E Int J, Ser B* 49(2):287–295. <https://doi.org/10.1299/jsmeb.49.287>
11. Dhurandhar SK, Sinha SL, Verma SK (2020) Effects of mixing vane spacer on flow and thermal behavior of fluid in fuel channels of nuclear reactors - a review. *Nucl Technol* 206:663–696. <https://doi.org/10.1080/00295450.2019.1698257>
12. Dhurandhar SK, Sinha SL, Verma SK (2022) Numerical evaluation for spacer vane effects on flow and heat transfer of water at supercritical pressure in annular channel. *Nucl Sci Eng* 196(5):600–613. <https://doi.org/10.1080/00295639.2021.2003650>
13. Dhurandhar SK, Sinha SL, Verma SK (2022) Spacer effects on thermal-hydraulic performance of fluid flow at supercritical pressure in annular channel-CFD methodology. *J Mech Eng Sci.* 16(1):8770–8787. <https://doi.org/10.15282/jmes.16.1.2022.10.0693>
14. Dhurandhar SK, Sinha SL, Verma SK (2019) Investigation of ring type spacer effects on performance of heat transfer and flow behaviour of supercritical r-134a flow using CFD in an annular channel. *Int J Adv Trends Comp Appl* 1(1):7–13
15. Dhurandhar SK, Sinha SL, Verma SK (2023) Numerical simulation to study mixing vane spacer effects on heat transfer performance of supercritical pressure fluid in an annular channel. *J Therm Eng* 9(6):1428–1441. <https://doi.org/10.18186/thermal.1395460>
16. Arai T, Ui A, Furuya M, Okawa R, Iiyama T, Ueda S, Shirakawa K (2023) Effect of non-heated rod arrangements on void fraction distribution in a rod bundle in high-pressure boiling flow. *Nucl Eng Des* 402:112101. <https://doi.org/10.1016/j.nucengdes.2022.112101>
17. Williams CL, Peterson AC Jr (2017) Two-phase flow patterns with high-pressure water in a heated four-rod bundle. *Nucl Sci Eng* 68:155–169. <https://doi.org/10.13182/NSE78-A27286>
18. Ren QY, Pan LM, Pu Z, Zhu F, He H (2021) Two-group phase distribution characteristics for air-water flow in 5 × 5 vertical rod bundle channel with mixing vane spacer grids. *Int J Heat Mass Transf* 176:121444. <https://doi.org/10.1016/j.ijheatmasstransfer.2021.121444>
19. Drucker MI, Dhir VK, Duffey RB (1984) Two-phase heat transfer for flow in tubes and over rod bundles with blockages. *J Heat Transfer* 106(4):856–864. <https://doi.org/10.1115/1.3246764>
20. Li J, Zhang C, Zhang Q, Yang P, Gan F, Chen S, Xiong Z, Xiao Y, Gu H (2022) Experimental investigation on onset of nucleate boiling and flow boiling heat transfer in a 5 × 5 rod bundle. *Appl Therm Eng* 208:118263. <https://doi.org/10.1016/j.applthermaleng.2022.118263>
21. Xiao Y, Duan TC, Ren QY, Zheng XY, Zheng M, He R (2022) Modeling and simulation analysis on mixing characteristics of two-phase flow around spacer grid. *Front Energy Res* 10:891074. <https://doi.org/10.3389/fenrg.2022.891074>
22. Yang X, Schlegel JP, Liu Y, Paranjape S, Hibiki T, Ishii M (2013) Experimental study of interfacial area transport in air-water two phase flow in a scaled 8 × 8 BWR rod bundle. *Int J Multiphase Flow* 50:16–32. <https://doi.org/10.1016/j.ijmultiphaseflow.2012.10.006>
23. Tian XW, Kui Z, Hou Y, Zhang Y (2016) Hydrodynamics of two-phase flow in a rod bundle under cross-flow condition. *Ann Nucl Energy* 91:206–214. <https://doi.org/10.1016/j.anucene.2016.01.025>
24. Hosokawa S, Hayashi K, Tomiyama A (2014) Void distribution and bubble motion in bubbly flows in a 4 × 4 rod bundl. Part I: Experiments. *J Nucl Sci Technol* 51:220–230. <https://doi.org/10.1080/00223131.2013.862189>
25. Inoue A, Kurosu T, Aoki T, Yagi M, Mitsutake T, Morooka S (1995) Void fraction distribution in BWR fuel assembly and evaluation of subchannel code. *J Nucl Sci Technol* 32(7):629–640. <https://doi.org/10.1080/18811248.1995.9731754>
26. ANSYS Inc (2013) Fluent R15 User's Theory Guide Release
27. Schiller L, Naumann Z (1935) A drag coefficient correlation. *Z Ver Deutsch Ing* 77:318–320
28. Tomiyama A (1998) Struggle with computational bubble dynamics. *Multiph Sci Technol* 10(4):369–405. <https://doi.org/10.1615/MultScienTechn.v10.i4.40>
29. Antal SP, Lahey RT, Flaherty JE (1991) Analysis of phase distribution in fully developed laminar bubbly two-phase flow. *Int J Multiph Flow* 17(5):635–652. [https://doi.org/10.1016/0301-9322\(91\)90029-3](https://doi.org/10.1016/0301-9322(91)90029-3)
30. Lopez de Bertodano M (1991) Turbulent bubbly flow in a triangular duct. Rensselaer Polytechnic Institute, Troy, New York.
31. Nikuradse J (1966) Laws of turbulent flow in smooth pipes. NASA TT F-10, 359. (English Translation)
32. Podila K, Rao Y (2016) CFD modelling of turbulent flows through 5 × 5 fuel rod bundles with spacer-grids. *Ann Nucl Energy* 97:86–95. <https://doi.org/10.1016/j.anucene.2016.07.003>
33. Liu CC, Ferng YM, Shih CK (2012) CFD evaluation of turbulence models for flow simulation of the fuel rod bundle with a spacer assembly. *Appl Therm Eng* 40:389–396. <https://doi.org/10.1016/j.applthermaleng.2012.02.027>
34. Cheng S, Chen H, Zhang X (2017) CFD analysis of flow field in a 5 × 5 rod bundle with multi-grid. *Ann Nucl Energy* 99:464–470. <https://doi.org/10.1016/j.anucene.2016.09.053>
35. Sohag FA, Mohanta L, Cheung FB (2017) CFD analyses of mixed and forced convection in a heated vertical rod bundle. *Appl Therm Eng* 117:85–93. <https://doi.org/10.1016/j.applthermaleng.2012.02.027>
36. Xiao Y, Li J, Deng J, Gao X, Pan GuH, J, (2020) Study of spacer effects on deteriorated heat transfer of supercritical fluid flow in an annulus. *Prog Nucl Energy* 123:103306. <https://doi.org/10.1016/j.pnucene.2020.103306>
37. Jaromin M, Anglart H (2013) A numerical study of heat transfer to supercritical water flowing upward in vertical tubes under normal and deteriorated conditions. *Nucl Eng Des* 264(11):61–70. <https://doi.org/10.1016/j.nucengdes.2012.10.028>
38. Cheng H, Zhao J, Rowinski MK (2017) Study on two wall temperature peaks of supercritical fluid mixed convective heat transfer in circular tubes. *Int J Heat Mass Transf* 113:257–267. <https://doi.org/10.1016/j.ijheatmasstransfer.2017.05.078>

39. Wang Y, Ferng YM, Sun LX (2019) CFD assist in design of spacer-grid with mixing-vane for a rod bundle. *Appl Therm Eng* 149:565–577. <https://doi.org/10.1016/j.applthermaleng.2018.12.090>
40. Dhurandhar SK, Sinha SL, Verma SK (2024) Numerical analysis for effects of grid spacer vane on flow-thermal characteristics of two phase flow in a 5 x 5 rod bundle. *Multiph Sci Technol* 36(3):19–44. <https://doi.org/10.1615/MultScienTechn.2024051035>

Publisher's Note

Springer Nature remains neutral with regard to jurisdictional claims in published maps and institutional affiliations.